Chinese Chemical Letters 31 (2020) 1598–1602

Contents lists available at ScienceDirect

Chinese Chemical Letters

journal homepage: www.elsevier.com/locate/cclet

Communication

Stepwise construction of Pt decorated oxygen-deficient mesoporous titania microspheres with core-shell structure and magnetic separability for efficient visible-light photocatalysis

Zhijian Li[b,1], Yao Wang[a,1], Ahmed A. Elzatahry[c], Xuanyu Yang[a], Shouzhi Pu[b], Wei Luo[d], Xiaowei Cheng[a,*], Yonghui Deng[a]

[a] Department of Chemistry, State Key Laboratory of Molecular Engineering of Polymers, Shanghai Key Laboratory of Molecular Catalysis and Innovative Materials, iChEM, Fudan University, Shanghai 200433, China
[b] Jiangxi Key Laboratory of Organic Chemistry, Jiangxi Science and Technology Normal University, Nanchang 330013, China
[c] Materials Science and Technology Program, College of Arts and Sciences, Qatar University, Doha PO Box 2713, Qatar
[d] State Key Laboratory for Modification of Chemical Fibers and Polymer Materials, College of Materials Science and Engineering, Donghua University, Shanghai 201620, China

ARTICLE INFO

Article history:
Received 21 September 2019
Received in revised form 15 October 2019
Accepted 18 October 2019
Available online 22 October 2019

Keywords:
Core-shell
Mesoporous TiO_2
Photocatalytic activity
Magnetic recovery
Visible light

ABSTRACT

Solid photocatalysts with high specific surface area, superior photoactivity and ease of recycling are highly desired in chemical process, water treatment and so on. In this study, a facile stepwise sol-gel coating approach was utilized to synthesize Pt decorated oxygen-deficient mesoporous titania microspheres with core-shell structure and convenient magnetic separability (denoted as Fe_3O_4@SiO_2@Pt/mTiO_{2-x}). These photocatalysts consist of magnetic Fe_3O_4 cores, nonporous insulating SiO_2 middle layer and mesoporous anatase TiO_{2-x} shell decorated by Pt nanoparticles (~3.5 nm) through wet impregnation and H_2 reduction. As a result of high activity of oxygen-deficiency of black TiO_{2-x} by H_2 reduction and efficient inhibition of electron-hole recombination by Pt nanoparticles, the rationally designed core-shell Fe_3O_4@SiO_2@Pt/mTiO_{2-x} photocatalysts exhibit superior photocatalytic performance in rhodamine B (RhB) degradation under visible light irradiation, with more than 98% of RhB degraded within 50 min. These core-shell structured photocatalysts show excellent recyclability under the assistance of magnetic separation with well-retained photocatalytic performance even after running five cycles. This stepwise synthesis method paves the way for the rational design of a high-efficiency recyclable heterogeneous catalyst, including photocatalysts, for various applications.

In recent years, more and more severe effects of water pollution to the environment and human health have aroused the extensive attention [1]. Among all the pollutants in wastewater, the dyestuff organics discharged from printing and dyeing industries are considered to be the most refractory ones, exhibiting the characteristics of high toxicity, potential carcinogenicity and difficult degradation [2,3]. Therefore, a great number of methodologies, such as advanced oxidation processes [4], enzymatic degradation [5], photocatalytic degradation [2,4,6,7], have been developed to reduce such environmental organic hazards. Compared to other methods for eliminating organic pollutants in wastewater, the photocatalytic degradation pathway possesses many attractive advantages including facile operations, low cost and good sustainability, which is highlighted as one of the most promising and environmental-friendly techniques in handling the increasing water pollutants under the irradiation of ultraviolet light or even visible light [2,4,6,8]. Titanium dioxide (TiO_2), as a wide-band-gap semiconducting metal oxide (band gap energy of 3.0–3.2 eV), is widely used in the fields of energy storage [9,10] and photocatalysis [11–14], mainly due to its intrinsic properties of high photocatalytic efficiency, good chemical stability, low cost and nontoxicity to environment. However, one of the most prominent limits of pure TiO_2 photocatalysts is the relatively low utilization of visible light because of their wide band gap and the quick recombination of photogenerated electron-hole pairs, which are produced by exciting the valence band electrons of TiO_2 into the conduction band by absorption of ultraviolet light.

* Corresponding author.
E-mail address: xwcheng@fudan.edu.cn (X. Cheng).
[1] These authors contributed equally to this work.

https://doi.org/10.1016/j.cclet.2019.10.016

Therefore, in order to enhance the photocatalytic activity of TiO_2 under visible light irradiation, a large number of modification strategies have been extensively explored, such as decoration with noble metals (Au, Pt, Pd, *etc.*) [12,13,15–19], doping with non-metals (C, N, F, S, B, *etc.*) [20,21], mixing two TiO_2 phases among anatase, rutile and brookite [14], creation of amorphous peroxo-TiO_2, *etc.* [22]. Besides, the design of functional photocatalysts with suitable morphologies and large surface area, such as core-shell or yolk-shell nanostructures [12,17,23], nanofibers [14], mesoporous structures [15,18], hollow thin sheets [24], hollow spheres [25,26], nanotubes [16] and so on, is another strategy to precisely adjust the migration distance of electrons and holes, which can distinctly improve the photocatalytic efficiency. Thus, it is acceptably recognized that a high-performance photocatalyst used under visible light can be rationally synthesized through combining more than one methodology described above.

Although the nanoscale functional photocatalysts based on TiO_2 show the promising catalytic efficiency in degradation of organics under visible light irradiation, they still suffer the unavoidable drawbacks of difficult separation and recycling from the heterogeneous catalysis systems [17]. In past decades, magnetite (Fe_3O_4) nanoparticles have attracted a great deal of interest because of their super paramagnetic property that is beneficial to their recovery usage under an external magnetic field [27]. Core-shell microspheres consisting of magnetic core and mesoporous outer shell are being developed as an important kind of recyclable composite heterogeneous catalysts [28]. However, the magnetic photocatalysts synthesized by directly coating TiO_2 onto magnetite particles showed a decreased photoactivity, due to an increase of electron-hole recombination caused by the unfavorable hetero-junction between TiO_2 shells and iron oxide cores [26]. The insulator polyelectrolytes were found to act as the corrosion protective membrane and prohibit the negative influence of iron oxide on photocatalysis [29]. In a photocatalyst of core-shell Fe_3O_4/SiO_2/polythiophene submicron composite, the specific semiconductor/insulator/semiconductor structure was highlighted to be helpful for the separation of photo-electrons and holes due to the introduction of SiO_2 as the insulating shell, and the catalytic efficiency of methyl orange photodegradation was greatly enhanced [23], but the UV light irradiation and the oxidizing agent of H_2O_2 were still needed for the catalytic reaction.

Herein, we reported the photocatalytic performance of magnetic core-shell oxygen-deficient titania microspheres (Fe_3O_4@SiO_2@Pt/mTiO_{2-x}) for the first time, which were obtained by a simple stepwise sol-gel coating strategy and further modified with Pt nanoparticles. The unique core-shell structure of magnetic Fe_3O_4 cores, nonporous SiO_2 insulating layers and oxygen-deficient mesoporous anatase TiO_{2-x} shells containing highly dispersed Pt nanoparticles endows the catalyst with significantly increased photocatalytic activity under visible light irradiation and superior recyclability, when used in photodegradation of organic pollutants and dyes (*e.g.*, RhB).

Scheme 1 illustrates the synthesis strategy of core-shell structured Fe_3O_4@SiO_2@Pt/mTiO_{2-x} microspheres. Firstly, using the classical Stöber method, uniform nonporous SiO_2 was deposited on magnetic Fe_3O_4 nanoparticles to obtain the core-shell Fe_3O_4@SiO_2 microspheres through the controlled hydrolysis and condensation of TEOS in ethanol/water/NH_4OH mixed solution. Secondly, a compact amorphous TiO_2 layer was coated on the surface of Fe_3O_4@SiO_2 by a similar sol-gel method *via* controlling the hydrolysis and condensation of TBOT. Thirdly, calcination in N_2 atmosphere at 400 °C was conducted to promote TiO_2 crystallization and mesopore formation in the shell, leading to the production of core-shell Fe_3O_4@SiO_2@mTiO_2 microspheres. Finally, with the treatment of wet impregnation and H_2 reduction, Pt nanoparticles were decorated inside mesopores of TiO_2 shells,

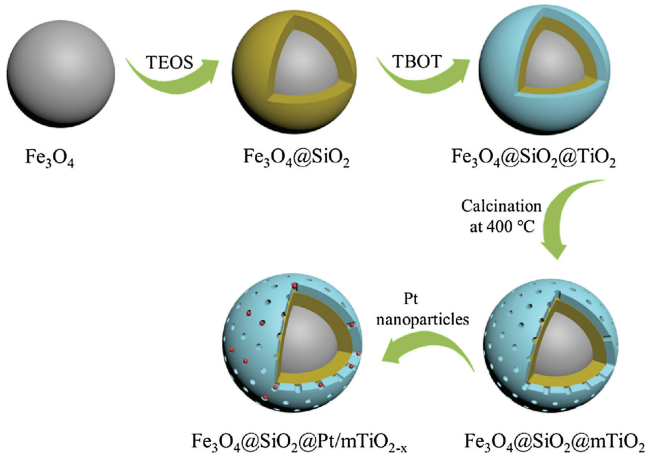

Scheme 1. Illustration of the synthesis procedure of Fe_3O_4@SiO_2@Pt/mTiO_{2-x} microspheres.

and at the same time TiO_2 was partially reduced to black TiO_{2-x}, to obtain the photocatalysts of Fe_3O_4@SiO_2@Pt/mTiO_{2-x} microspheres.

X-ray diffraction (XRD) pattern of the as-prepared Fe_3O_4 particles displays six well-resolved diffraction peaks centered at 30.4°, 35.6°, 43.3°, 53.7°, 57.3° and 62.7°/2θ (Fig. 1a), which are indexed to (220), (311), (400), (422), (511) and (440) reflections of the typical cubic Fe_3O_4 (JCPDS card No. 190629) [30]. After coating SiO_2 on Fe_3O_4 surface, the pattern containing six diffraction peaks in Fe_3O_4@SiO_2 is quite similar to that of the parent Fe_3O_4 microspheres, but a broad peak at around 22°/2θ appears, which is corresponding to the amorphous SiO_2 phase (Fig. 1b) [31]. Without calcination, the deposited TiO_2 shell still shows the amorphous phase in Fe_3O_4@SiO_2@TiO_2 (Fig. S1 in Supporting information). Calcination at 400 °C promotes TiO_2 crystallization into anatase phase with the characteristic diffraction peaks at 25° and 48°/2θ (Fig. 1c), that can be assigned to the (101) and (200) crystal planes of anatase TiO_2 (JCPDS card No. 21-1272) [32], indicating that crystallized TiO_2 was successfully coated on Fe_3O_4@SiO_2. Nevertheless, after decorating Pt nanoparticles by wet impregnation and H_2 reduction, the diffraction pattern of Fe_3O_4@SiO_2@Pt/mTiO_{2-x} remains unchanged, and no diffraction peaks about Pt nanoparticles were detected (Fig. 1d), which may be due to their low loading content and high dispersity in TiO_{2-x} layer.

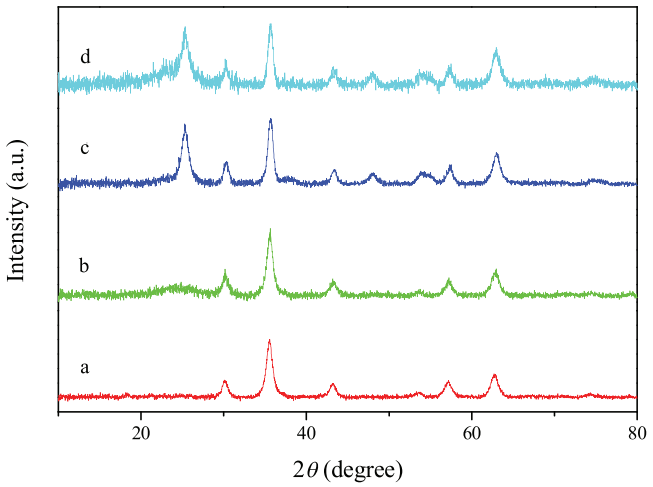

Fig. 1. XRD patterns of (a) Fe_3O_4, (b) Fe_3O_4@SiO_2, (c) Fe_3O_4@SiO_2@mTiO_2 and (d) Fe_3O_4@SiO_2@Pt/mTiO_{2-x} composites.

Using the solvothermal synthesis method, we have synthesized the hydrophilic magnetic Fe_3O_4 particles, which present the uniform spherical morphology with a mean diameter of 200 nm (Fig. S2A in Supporting information). These particles actually consist of a great number of magnetite nanocrystals in size of about 10 nm, so they have rough surface and pomegranate-like microstructures with superparamagnetic property. Notably, the surface of Fe_3O_4 particles is anchored with a great number of citrate groups, thus they can be well dispersed in polar solvents of water and ethanol, which is conductive to the subsequent deposition of silica layer. After controllable hydrolysis and condensation of TEOS through a sol-gel process, a nonporous SiO_2 layer was uniformly coated on Fe_3O_4 particles to form the core-shell Fe_3O_4@SiO_2 microspheres, presenting spherical morphology but much smoother surface and larger particle size of about 300 nm (Fig. S2B in Supporting information). TEM images indicate that the thickness of the silica shell is around 50 nm (Figs. 2A and B), in good consistence with the SEM image in Fig. S2B. As a transitional and protective layer, the SiO_2 shell provides an appropriate interface for following deposition of TiO_2 layer, and it can also enhance the stability and reusability of Fe_3O_4 particles and promote the photocatalytic activity of TiO_2 by decreasing the adverse influence of Fe_3O_4 cores. Under the similar sol-gel coating procedure and followed calcination treatment, the second layer of anatase TiO_2 was controllably deposited on SiO_2 surface, leading to the well-defined Fe_3O_4@SiO_2@mTiO_2 microspheres with much larger particle diameter of ~340 nm but rough surface (Fig. S2C in Supporting information), mainly due to faster hydrolysis and condensation rate of TBOT than TEOS and formation of crystallized TiO_2 nanoparticles by calcination. TEM images in Figs. 2A and B clearly reveal the typical three-layer sandwich structure of Fe_3O_4@SiO_2@mTiO_2, which consists of a dark Fe_3O_4 core, a light-colored silica interlayer and a TiO_2 shell with rough surface and thickness of around 20 nm. Notably, the TiO_2 layer is composed of numerous highly crystallized nanocrystals with the lattice spacing of 0.316 nm (Fig. 2C), assigned to the (101) plane of anatase TiO_2 [33], and the disordered mesopores are ascribed to the voids aggregated by these nanoparticles. After decorating Pt nanoparticles through wet impregnation and H_2 reduction, the sample of Fe_3O_4@SiO_2@Pt/mTiO_{2-x} still shows the spherical morphology, uniform particle size and good dispersibility (Fig. S2D in Supporting information). From TEM images of Figs. 2D and E, it can be seen that Pt nanoparticles of ~3.5 nm in size are highly dispersed inside the mesoporous TiO_{2-x} shells. The energy-dispersive X-ray spectroscopy (EDX) spectrum confirms the existence of Fe, Si, Ti and Pt elements in these core-shell microspheres (Fig. 2F), in which Pt content is calculated to be about 1.45%.

X-ray photoelectron spectroscopy (XPS) was used to examine the compositions and valence states of surface elements in Fe_3O_4@SiO_2@Pt/mTiO_{2-x}, in which the elements of O, Si, Ti and Pt could be detected but no peaks about Fe element appear (Fig. 3A), proving that the magnetic Fe_3O_4 core is well encapsulated inside the core-shell microspheres. Two main peaks centered at 458.2 and 464.1 eV (Fig. 3B) can be assigned to the Ti^{4+} $2p_{3/2}$ and Ti^{4+} $2p_{1/2}$, respectively. In addition, two additional peaks at 456.7 and 462.8 eV can be attributed to Ti^{3+} $2p_{3/2}$ and Ti^{3+} $2p_{1/2}$ respectively [34–36], revealing the existence of Ti^{3+} in the shell with Ti^{3+}/Ti^{4+} ratio as high as 0.72. The result demonstrates that most of the tetravalent titanium was reduced to Ti^{3+} through H_2 treatment at high temperature, which can greatly suppress the recombination of photoinduced electron-hole pairs and promote charge separation [37], thus enhancing the photocatalytic activity of the core-shell microspheres. Two fitted peaks at 75.5 and 72.2 eV demonstrate the production of Pt^0 $4f_{5/2}$ and Pt^0 $4f_{7/2}$, respectively (Fig. 3C), which indicates that Pt nanoparticles reduced by H_2 treatment are uniformly decorated in TiO_{2-x} shells [38].

Fig. S3A (Supporting information) shows the nitrogen adsorption-desorption isotherm curves of Fe_3O_4@SiO_2@mTiO_2 and Fe_3O_4@SiO_2@Pt/mTiO_{2-x}, both of which display Type IV isotherm with an obvious hysteresis loop, indicating the formation of well-developed mesopores in the core-shell structured samples [39]. The Brunauer-Emmett-Teller (BET) surface area and total pore volume of Fe_3O_4@SiO_2@Pt/mTiO_{2-x} are 72.4 m^2/g and 0.060 cm^3/g, respectively, quite close to those of Fe_3O_4@SiO_2@TiO_2 (69.2 m^2/g

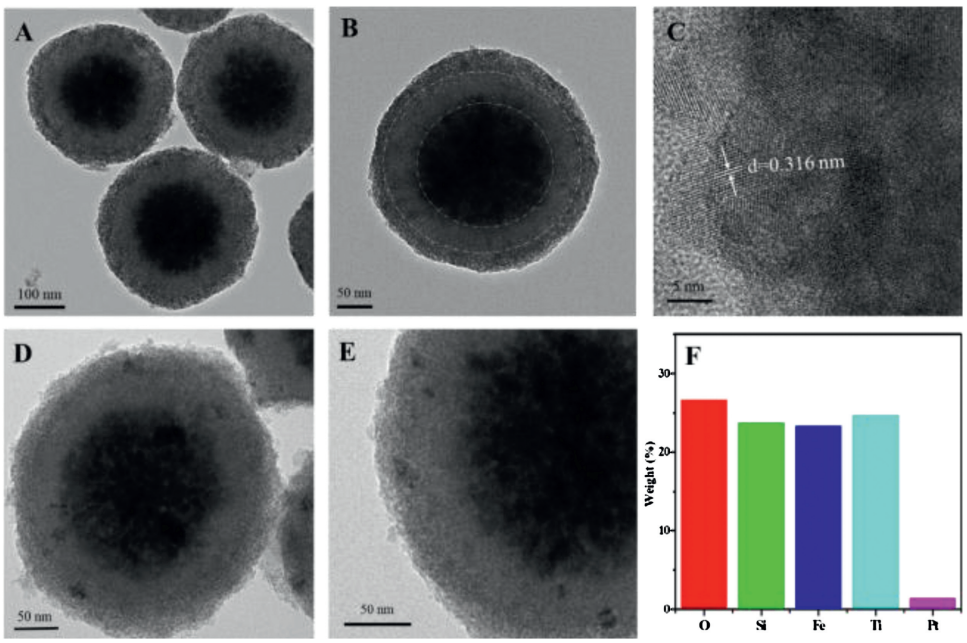

Fig. 2. TEM (A, B) and HRTEM images (C) of Fe_3O_4@SiO_2@mTiO_2; TEM images (D and E) and EDS spectrum (F) of Fe_3O_4@SiO_2@Pt/mTiO_{2-x}.

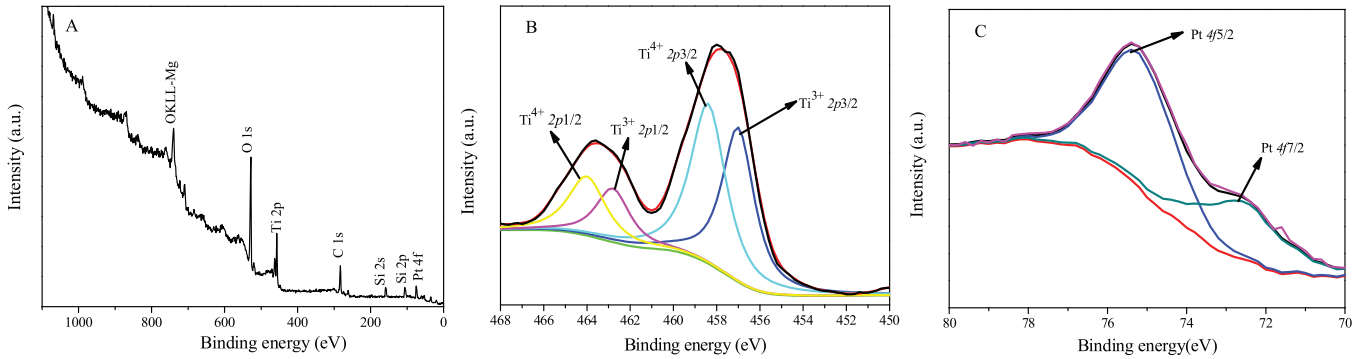

Fig. 3. XPS characterization of Fe_3O_4@SiO_2@Pt/mTiO_{2-x}. (A) XPS survey spectrum, (B) Ti 2p spectrum and (C) Pt 4f spectrum.

and 0.057 cm^3/g). The pore size distributions derived from the adsorption branches of the isotherms by using Barrett-Joyner-Halenda (BJH) model display a mean pore size of around 4.5 nm for both samples (Fig. S3B in Supporting information), indicating that the mesopores in TiO_2 shell are completely open even after loading Pt nanoparticles, which can effectively contribute to fast adsorption and mass diffusion during the photocatalytic reaction.

Due to the intrinsic magnetic property and the unique core-shell structure with high surface area and Pt-decorated oxygen-deficient mesoporous TiO_{2-x}, it is believed that the sample of Fe_3O_4@SiO_2@Pt/mTiO_{2-x} may have a potential use as the photocatalyst for RhB degradation under visible light irradiation, in comparison with the catalytic performance of Fe_3O_4@SiO_2 and Fe_3O_4@SiO_2@mTiO_2 under the same evaluation conditions (Fig. 4). The Fe_3O_4@SiO_2 core-shell hybrids show a negligible adsorption of RhB without visible light irradiation (in dark), mainly due to the low adsorption capacity of nonporous SiO_2 shell. Whereas, both Fe_3O_4@SiO_2@mTiO_2 and Fe_3O_4@SiO_2@Pt/mTiO_{2-x} give an obvious increase in RhB adsorption, because of large surface area of the deposited mesoporous TiO_2 shells and their strong affinity with RhB. Under the visible light irradiation, the Fe_3O_4@SiO_2@Pt/mTiO_{2-x} core-shell hybrids exhibit the best catalytic performance with RhB degradation efficiency up to 98% within 50 min (Fig. 4A, curve c and Fig. S4B in Supporting information). For comparison, Fe_3O_4@SiO_2 and Fe_3O_4@SiO_2@mTiO_2 can only convert 24% and 55% of RhB under the same conditions, respectively (Fig. 4A, curves a and b and Fig. S4A in Supporting information), indicating that the photocatalytic activity can be significantly enhanced by coating highly crystallized mesoporous anatase TiO_{2-x} shell and decorating Pt nanoparticles as well. It is well known that most of the photocatalytic reactions can be fitted with the typical Langmuir-Hinshelwood model [4], and here the equation of $\ln(C_0/C) = kt$ is adopted to calculate the apparent rate constant (k), where C_0 and C are the initial concentration and the concentration of RhB at different exposed time, respectively. The k value of RhB degradation for Fe_3O_4@SiO_2@Pt/mTiO_{2-x} is calculated to be 0.0942 min^{-1} (Fig. 4B), which is 24.5 and 5.71 times higher than that of Fe_3O_4@SiO_2 (0.00384 min^{-1}) and Fe_3O_4@SiO_2@mTiO_2 (0.0165 min^{-1}), respectively, further indicating the superior photocatalytic performance of the Fe_3O_4@SiO_2@Pt/mTiO_{2-x} core-shell hybrids towards RhB degradation.

The stability and reusability of catalysts for continuous degradation of organics are quite important for practical application in industry. Five-cycle experiments were conducted to demonstrate the recyclability of Fe_3O_4@SiO_2@Pt/mTiO_{2-x} for RhB photodegradation in Fig. S5 (Supporting information). In each run, the photocatalyst can stably receive higher than 98% of degradation efficiency within 50 min, which was then completely and quickly separated from the aqueous solution held in an applied magnetic field for the consecutive catalytic evaluations. After five cycles of photocatalytic determinations, there was no significant loss of catalytic activity and magnetic strength even under visible light irradiation longer than the total exposed time of 250 min, indicating that the Fe_3O_4@SiO_2@Pt/mTiO_{2-x} core-shell microspheres are very stable and highly reactive with a long life time during the photocatalytic test.

Fig. S6 (Supporting information) describes the mechanism of photocatalytic degradation of RhB over oxygen-deficient

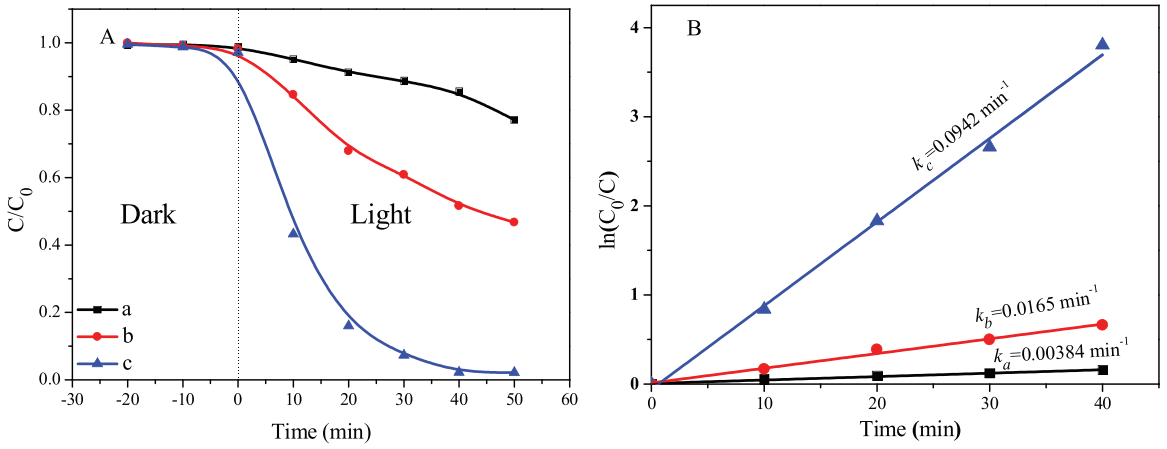

Fig. 4. (A) Photocatalytic degradation performance of RhB on various core-shell structured catalysts; (B) *Pseudo*-first-order linear relationship between reaction time and ln (C_0/C), where C_0 and C represent the initial concentration and the concentration of RhB at different exposed time, respectively: Fe_3O_4@SiO_2 (a), Fe_3O_4@SiO_2@mTiO_2 (b) and Fe_3O_4@SiO_2@Pt/mTiO_{2-x} (c).

Fe_3O_4@SiO_2@Pt/mTiO_{2-x} microspheres under visible light irradiation. At first, the irradiation of visible light can inspire the generation of conduction band electrons (e^-) and valence band holes (H^+) of TiO_{2-x} in mesoporous shell. Due to the effective combination of highly-dispersed Pt nanoparticles and partially-reduced anatase TiO_{2-x}, the photogenerated electrons in the conduction bands can easily transfer to the Pt surface, which greatly prohibits the electron-hole recombination rate. Then O_2 molecules capture electrons from the surface of Pt nanoparticles, to form the highly active O_2^- species, which can quickly oxidize organics into CO_2 and water. From the mechanism investigation, the excellent photocatalytic performance of Fe_3O_4@SiO_2@Pt/mTiO_{2-x} photocatalyst can be attributed to the following characteristics: (1) The mesoporous structure of thin TiO_{2-x} shell, which is beneficial for the adsorption and diffusion of large organic molecules; (2) High crystallization of the TiO_{2-x} layer, which contains rich defects and active sites exposed to reactants; (3) The loaded Pt nanoparticles could act as the electron traps to facilitate the separation of photogenerated electron-hole pairs and promote the electron transfer process between the interface of TiO_{2-x} and Pt; (4) The silica interlayer and magnetic Fe_3O_4 core can enhance the stability and recyclability of the photocatalyst, respectively.

In summary, we report a conventional stepwise sol-gel coating approach to synthesize the magnetic core-shell Fe_3O_4@SiO_2@m-TiO_2 microspheres, which exhibit the novel three-layer sandwich structure containing Fe_3O_4 cores of ~200 nm in diameter, nonporous SiO_2 insulating layers of about 50 nm in thickness and mesoporous anatase TiO_2 shells of 4.5 nm in pore size and 20 nm in thickness. Using the facile wet impregnation and H_2 reduction routes, the magnetic core-shell photocatalyst of oxygen-deficient Fe_3O_4@SiO_2@Pt/mTiO_{2-x} nanocomposites were obtained by uniform decoration of Pt nanoparticles in size of ~3.5 nm within the mesopores of TiO_{2-x} shells, which were formed by TiO_2 reduction combined with Pt deposition through H_2 treatment. The photocatalytic activity of the core-shell Fe_3O_4@SiO_2@Pt/mTiO_{2-x} microspheres was evaluated by RhB degradation under visible light irradiation, and the photocatalytic efficiency can exceed 98% within 50 min, showing the highest k in comparison with other core-shell nanocomposites of Fe_3O_4@SiO_2 and Fe_3O_4@SiO_2@m-TiO_2. The recycling experiments indicate the promising stability and reusability in RhB photodegradation. The catalytic mechanism based on this core-shell Fe_3O_4@SiO_2@Pt/mTiO_{2-x} photocatalyst was supposed to further interpret the superior photocatalytic performance, which mainly originates from the magnetic core-shell structures and the synergistic effects of uniformly dispersed Pt nanoparticles, highly crystallized mesoporous anatase TiO_{2-x} and nonporous SiO_2 transitional layer.

Declaration of competing interest

The authors declare that they have no known competing financial interests or personal relationships that could have appeared to influence the work reported in this paper.

Acknowledgments

This work was supported by the National Natural Science Foundation of China (Nos. 51372041, 51422202, 21673048, 21875044, 51822202 and 51772050), Key Basic Research Program of Science and Technology Commission of Shanghai Municipality (No. 17JC1400100), Youth Top-notch Talent Support Program of China, Shanghai Rising-Star Program (No. 18QA1400100) and DHU Distinguished Young Professor Program.

Appendix A. Supplementary data

Supplementary material related to this article can be found, in the online version, at doi:https://doi.org/10.1016/j.cclet.2019.10.016.

References

[1] J.L. Martinez, Environ. Pollut. 157 (2009) 2893–2902.
[2] N. Pugazhenthiran, P. Sathishkumar, P. Maruthamuthu, S. Anandan, J. Porous Mater. 20 (2013) 489–499.
[3] M. Eisenstein, Nature 521 (2015) S52.
[4] L. Tang, Y. Liu, J. Wang, et al., Appl. Catal. B: Environ. 231 (2018) 1–10.
[5] S. Fang, X. An, H. Liu, et al., Bioresour. Technol. 185 (2015) 28–34.
[6] L. Qin, D. Huang, P. Xu, et al., J. Colloid Interface Sci. 534 (2019) 357–369.
[7] B. Huang, J. He, S. Bian, et al., Chin. Chem. Lett. 29 (2018) 1698–1701.
[8] Y. Lv, L. Yu, C. Li, L. Yang, Sci. Chin. Chem. 59 (2016) 142–149.
[9] X. Lu, G. Wang, T. Zhai, et al., Nano Lett. 12 (2012) 1690–1696.
[10] J. Du, J. Qi, D. Wang, Z. Tang, Energy Environ. Sci. 5 (2012) 6914–6918.
[11] J.B. Joo, Q. Zhang, I. Lee, et al., Adv. Funct. Mater. 22 (2012) 166–174.
[12] M. Wang, J. Han, H. Xiong, R. Guo, Langmuir 31 (2015) 6220–6228.
[13] S.I. Naya, A. Inoue, H. Tada, J. Am. Chem. Soc. 132 (2010) 6292–6293.
[14] D. Yang, H. Liu, Z. Zheng, et al., J. Am. Chem. Soc. 131 (2009) 17885–17893.
[15] J. Lu, P. Zhang, A. Li, et al., Chem. Commun. 49 (2013) 5817–5819.
[16] T. Yui, A. Kan, C. Saitoh, et al., ACS Appl. Mater. Interfaces 3 (7) (2011) 2594–2600.
[17] H. Liang, B. Zhang, H. Ge, et al., ACS Catal. 7 (2017) 6567–6572.
[18] H. Li, Z. Bian, J. Zhu, et al., J. Am. Chem. Soc. 129 (2007) 4538–4539.
[19] X. Li, J. Wang, M. Li, et al., Chin. Chem. Lett. 29 (2018) 527–530.
[20] R. Asahi, T. Morikawa, T. Ohwaki, et al., Science 293 (2001) 269–271.
[21] D. Chen, D. Yang, Q. Wang, Z. Jiang, Ind. Eng. Chem Res. 45 (2006) 4110–4116.
[22] J. Seo, H. Lee, H.J. Lee, et al., Appl. Catal. B: Environ. 225 (2018) 487–495.
[23] F. Zhang, Y. Shi, Z. Zhao, et al., Appl. Catal. B: Environ. 150–151 (2014) 472–478.
[24] W. Wang, D. Zhu, Z. Shen, et al., Ind. Eng. Chem. Res. 55 (2016) 6373–6383.
[25] H. Li, J. Li, Y. Zhu, et al., Anal. Chem. 90 (2018) 5496–5502.
[26] D. Beydoun, R. Amal, G.K.C. Low, S. McEvoy, J. Phys. Chem. B 104 (2000) 4387–4396.
[27] Y. Zhang, Q. Yue, L. Yu, et al., Adv. Mater. 30 (2018) e1800345.
[28] Y. Deng, D. Qi, C. Deng, et al., J. Am. Chem. Soc. 130 (2008) 28–29.
[29] V. Belessi, D. Lambropoulou, I. Konstantinou, et al., Appl. Catal. B: Environ. 87 (2009) 181–189.
[30] X.W. Lou, L.A. Archer, Adv. Mater. 20 (2010) 1853–1858.
[31] Y. Zhu, E. Kockrick, T. Ikoma, et al., Chem. Mater. 21 (2009) 2547–2553.
[32] S.D. Perera, R.G. Mariano, K. Vu, et al., ACS Catal. 2 (2012) 949–956.
[33] T. Yang, J. Peng, Y. Zheng, et al., Appl. Catal. B: Environ. 221 (2018) 223–234.
[34] J. Chen, W. Song, H. Hou, et al., Adv. Funct. Mater. 25 (2016) 6793–6801.
[35] G. Li, Z. Lian, X. Li, et al., J. Mater. Chem. 3 (2015) 3748–3756.
[36] S.T. Myung, M. Kikuchi, S.Y. Chong, et al., Energy Environ. Sci. 6 (2013) 2609–2614.
[37] S.H. Szczepankiewicz, J.A. Moss, M.R. Hoffmann, J. Phys. Chem. B 106 (2002) 2922–2927.
[38] J.S. Jang, S. Yu, S.J. Choi, et al., Small 12 (2016) 5989–5997.
[39] L. Pinho, M.J. Mosquera, J. Phys. Chem. C 115 (2011) 22851–22862.